2025 IEEE World Haptics Conference (WHC)
Suwon Convention Center, Suwon, Korea
July 8 ~ 11, 2025

Optical Fiber-based Force Myography (FMG) Sensor for Hand Gesture and Grasping Force Estimation

Chongyoung Chung
Dept. of Mechanical Engineering
Korea Advanced Institute of Science and Technology (KAIST)
Daejeon, South Korea
cy.chung@kaist.ac.kr

Heeju Mun
Dept. of Mechanical Engineering
Korea Advanced Institute of Science and Technology (KAIST)
Daejeon, South Korea
heeju.1234@kaist.ac.kr

Ki-Uk Kyung
Dept. of Mechanical Engineering
Korea Advanced Institute of Science and Technology (KAIST)
Daejeon, South Korea
kyungku@kaist.ac.kr

***Abstract*—This study presents the design, optimization, and evaluation of an optical fiber-based force myography (FMG) sensor for hand gesture and grasping force estimation, with potential haptic applications for realistic human-robot interaction (HRI). The sensor, with a diameter of 10 mm and a thickness of 2 mm, is designed to be flexible and easily integrated into clothing or sleeves. Utilizing the principle of light loss due to touch in bent optical fibers, the sensor demonstrates high sensitivity and stability. Through simulation, the sensor design parameters, such as the bending radius and the number of weavings, were optimized to achieve a high signal-to-noise ratio and sensitivity. The fabricated sensor showed excellent performance in various experiments, including high sensitivity, repeatability, and accurate force estimation. A wearable system with four embedded sensors achieved 91% hand gesture recognition accuracy using long short-term memory neural network and grasping force estimation exhibited high linearity across different ball grip types. These findings demonstrate the sensor practicality, with future research focusing on improving durability and exploring broader applications in haptics and HRI.**

Keywords*— *force sensor, optical fiber, force myography, gesture recognition, grasping force, human-robot interaction, haptics

I. Introduction

Robots are increasingly integrated into activities of daily living (ADL), extending their applications beyond traditional industrial environments. Accurate and intuitive human-robot interaction (HRI) is essential for enabling robots to perform tasks in close collaboration with humans. This interaction involves human motion recognition, which is essential for haptic applications in wearable robots [1], [2], prosthetic devices [3], [4], and virtual reality (VR) systems [5], [6]. Realistic haptic feedback requires not only accurate hand gesture recognition but also precise grasping force estimation to ensure an immersive and responsive user experience. To enable these capabilities, researchers have explored methods such as vision-based motion capture, wearable glove-type sensors, and bio-signal-based approaches.

This work was supported by the Institute of Information & Communications Technology Planning & Evaluation (IITP) by the Korea Government Ministry of Science and ICT (MSIT) (No. RS-2025-02303658). *(Corresponding author: Ki-Uk Kyung)*

This work involved human subjects or animals in its research. Approval of all ethics and experimental procedures and protocols was granted by the Institutional Review Board at the Korea Advanced Institute of Science and Technology (KH2024-118).

Vision-based motion capture is widely used for precision in tracking complex movements [7]. However, it requires multiple cameras and intricate setups to address blind spots, making it less suitable for portable or user-oriented systems. Wearable glove-type sensors provide high-resolution motion tracking but are bulky and can interfere with actuators in applications such as virtual haptics [8], [9]. Additionally, these methods are less effective for disabled individuals with amputations, as they rely on detecting physical joint movements. To overcome these limitations, bio-signal-based approaches, such as surface electromyography (sEMG) and force myography (FMG), have gained attention for their ability to measure muscle activity, even in cases of restricted motion.

sEMG, one of the most widely studied bio-signal-based techniques, detects electrical signals generated by muscle contractions [10]-[12]. While it provides valuable information in both time and frequency domains, the raw signals are inherently noisy and require extensive filtering and complex machine learning models for accurate interpretation. Additionally, sEMG is highly susceptible to factors such as skin impedance and electromagnetic interference (EMI), significantly limiting its usability in practical environments.

In contrast, FMG sensors measure changes in muscle force and are categorized into force-sensitive resistor (FSR)-based sensors, pneumatic sensors, and optical fiber-based sensors. FSR sensors are compact but suffer from drift and limited sensitivity [13], while pneumatic sensors offer high accuracy but lack durability due to imperfect air sealing of the air bladder [14]. Optical fiber-based FMG sensors, include strain and force sensors, known for their thin, lightweight designs and EMI immunity, have been explored using micro-bending structures for enhanced sensitivity and force detection ranges [15]-[19]. wever, these designs often require rigid frames to create micro-bending under external force, reducing wearability and durability during extended use.

To address these challenges, we propose a novel and sensitive FMG sensor utilizing woven optical fibers to enhance wearability, reliability, and performance under sweating conditions. The compact sensor, measuring 10 mm in diameter and 2 mm in thickness as shown in Fig. 1, offers flexibility and can be seamlessly integrated into wearable systems with minimal discomfort. Designed to detect forces within the

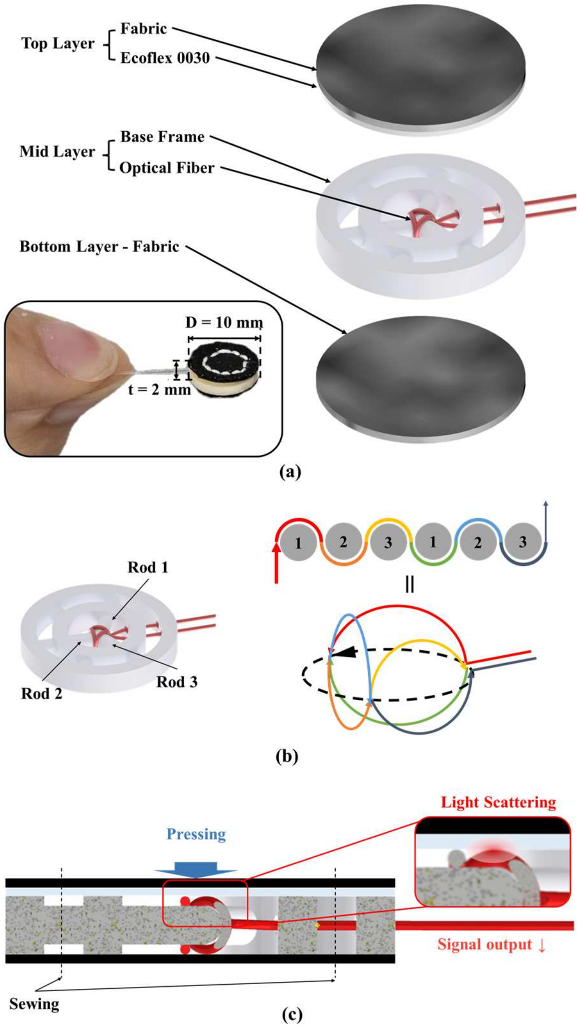

Figure 1. (a) Overall design of the optical fiber-based force myography sensor which has 10 mm of diameter and 2 mm of thickness. (b) Optical fiber was woven up and down on the rod. (c) The signal output decreases due to light scattering between the optical fiber and the polymer as the sensor is pressed.

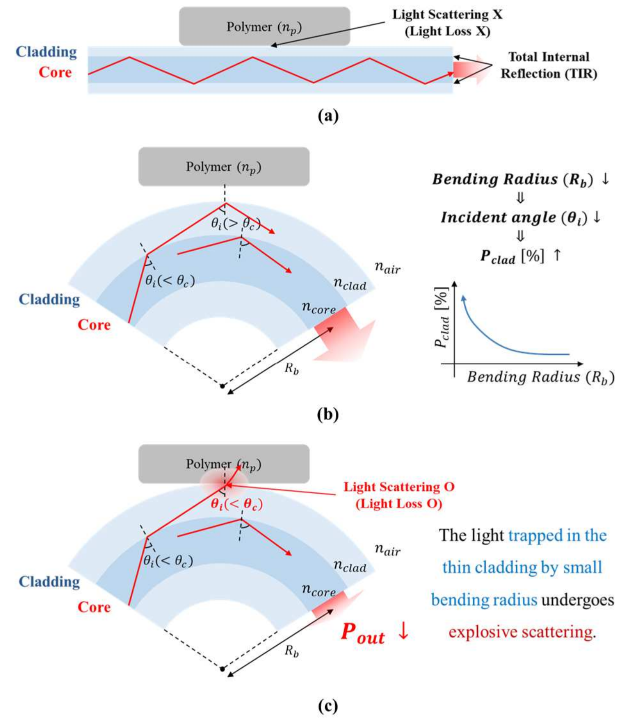

Figure 2. (a) For the optical fiber without bending, even though the optical fiber is touched by high refractive index polymer, there is no light scattering because of the total internal reflection (TIR) between cladding and core. (b) When the optical fiber is bent, some portion of the light begin to propagate through the cladding. (c) When the optical fiber is touched by polymer, the light in the cladding scatters which induces the light loss.

critical range of 3 N required for upper-limb FMG applications [20], the primary purpose of the sensor is to enable accurate hand gesture recognition. Additionally, as a secondary feature, the sensor demonstrates the capability to estimate grasping forces during object manipulation. A wearable system incorporating the sensor was developed to classify six distinct hand gestures with 91% accuracy using a Long Short-Term Memory (LSTM) neural network and to estimate grasping forces across different ball grips. These results demonstrate the potential of the sensor as a practical solution for both gesture recognition and grasping force estimation in wearable haptic applications.

II. Optical Fiber-based Sensor Design

A. Working Principle

In general, there is almost no light loss in the optical fiber without bending due to total internal reflection (TIR) as shown in Fig. 2(a). When the optical fiber is bent, the change in the incident angle causes part of the core-mode light to transition into cladding-mode as shown in Fig. 2(b) [21], [22]. When the cladding comes into contact with a material of higher refractive index, significant light loss occurs due to the scattering of cladding-mode light as shown in Fig. 2(c). This property makes optical fibers highly effective for detecting force or pressure by monitoring changes in light intensity.

To achieve consistent bending and thereby, maximizing amount of cladding-mode for high sensitivity, a weaving structure was adopted where the optical fiber was alternately woven onto a flexible base at regular intervals as shown in Fig. 1(b). This design increased the contact area between the fiber and the material, improving the sensitivity and efficiency of the sensor. The simplicity of this weaving approach, combined with its effectiveness in enhancing transition of core to cladding-mode, highlights its potential for various sensor applications.

B. Sensor Design Parameter Optimization

To improve the sensing performance of the scattering-based optical sensor, it was essential to determine the optimal design parameters. The two primary design parameters considered were the bending radius (R_b) and the number of weavings (N). As the R_b decreases, the light loss, transition of cladding-mode, increases due to the greater deflection of the optical fiber, leading to higher sensitivity. However, excessive bending also causes significant light leakage even before any external force is applied, which reduces the signal-to-noise ratio (SNR) and is called bending loss [23]. And, increasing N naturally enhances

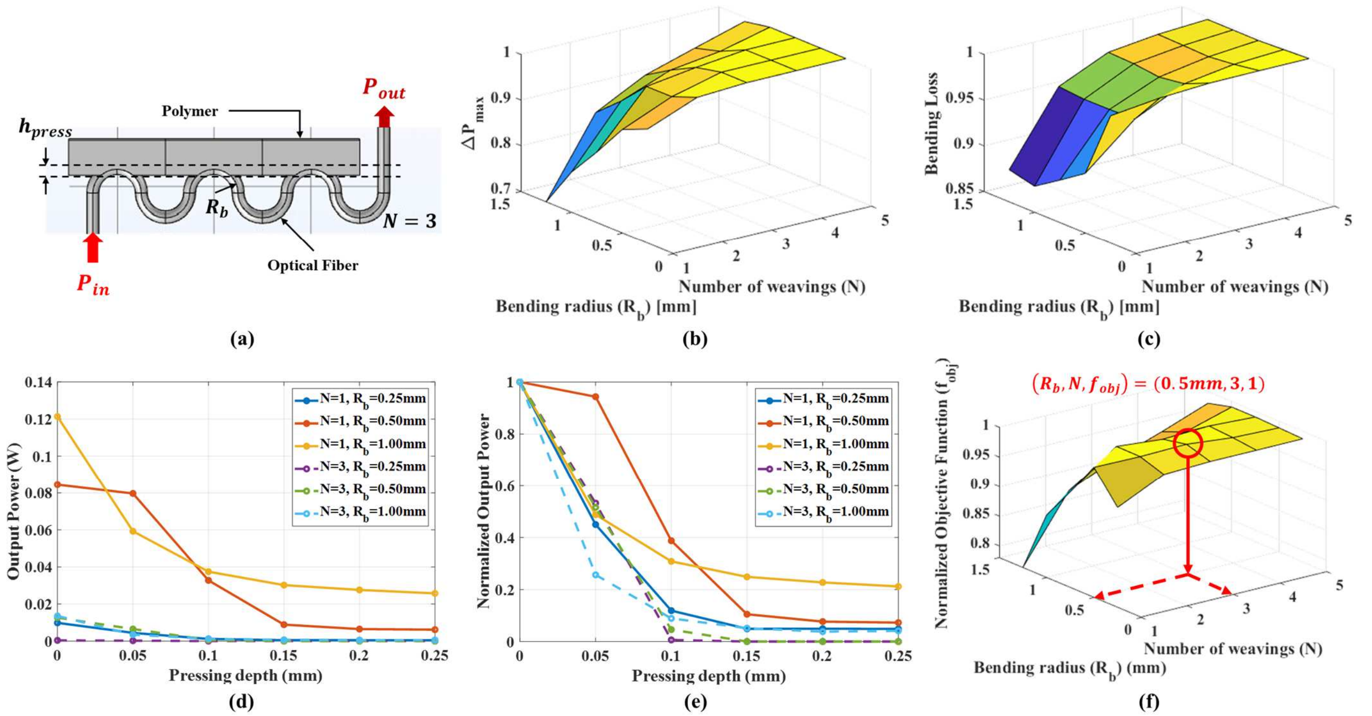

Figure 3. (a) Captured picture of COMSOL Simulation window. The optical fiber was uniformly woven, and the polymer was brought into contact with the woven sections, causing light scattering. The resulting changes in output power were then examined. Simulation results of (b) the normalized maximum power loss and (c) bending loss along with bending radius (R_b) and number of weavings (N). (d) The output power decreased as the sensor was pressed, due to light scattering. And the output power in the unpressed state is lowered when the N increases or R_b decreases. (e) The output power is normalized to 1 in the unpressed state. (f) Design parameters were optimized by objective function which are $(R_b, N) = (0.5\ mm, 3)$.

TABLE I. Parameters of COMSOL Simulation

Parameters	Value	Unit
Core refractive index (n_{core})	1.492	-
Cladding refractive index (n_{clad})	1.402	-
Air refractive index (n_{air})	1.000	-
Polymer refractive index (n_{pol})	1.670	-
Core diameter (d_{core})	240	µm
Cladding diameter (d_{clad})	250	µm
Wavelength (λ)	630	nm

the contact area between the fiber and the polymer, resulting in greater light loss and improved force detection. One the other hand, excessively increasing the value of N not only enlarges the sensor size but also makes it overly sensitive. These trade-offs necessitated a careful balance to maximize sensitivity while minimizing the initial bending loss.

Therefore, simulations (COMSOL Multiphysics) were conducted to evaluate the light loss characteristics of the optical fiber under varying R_b and N. In the simulation, an input power of 1 W (P_{in}) was applied to the woven optical fiber structure. Subsequently, the polymer layer was placed on the bent section of the optical fiber, as shown in Fig. 3(a), allowing the contact area with the polymer to be adjusted based on the pressing depth (h_{press}). Then, the bending loss was assessed by measuring the output power at the outlet, $P_{out}(R_b, N, h_{press})$, without applying any external touch using a polymer layer ($h_{press} = 0$). This allowed us to quantify the inherent light loss caused solely by the bending of the optical fiber. Subsequently, the polymer layer was progressively pressed with the bent section of the optical fiber by increasing h_{press} from 0 to 250 µm, and the changes in output power during the pressing were evaluated.

To identify the optimal R_b and N, an objective function (f_{obj}) was set which needs to be maximized, as shown in Equation (1)-(3). The objective function minimizes initial bending loss without touch to enhance SNR while maximizing the output power loss during contact with the polymer to improve sensitivity, where $\Delta\bar{P}_{max}$ is the normalized maximum power loss at the maximum press depth. Detailed information about the parameters is provided in TABLE. I.

$$f_{obj} = \frac{\Delta\bar{P}_{max}}{P_{in} - P_{out}} \propto \frac{Sensitivity}{Bending\ Loss} \tag{1}$$

$$\Delta\bar{P}_{max} = \frac{P_{out}(R_b, N, 0) - P_{out}(R_b, N, 250\mu m)}{P_{out}(R_b, N, 0)} \tag{2}$$

$$P_{in} - P_{out} = 1\ [W] - P_{out}(R_b, N, 0) \tag{3}$$

Based on the simulation results, as shown in Fig. 3 (b) and (c), it was observed that $\Delta\bar{P}_{max}$ and bending loss both increase as R_b decreases and N increases. This trend becomes clearer in Fig. 3(d), which compares the output power according to the pressing depth. The results indicate that larger N and smaller R_b lead to lower overall output power, which could negatively impact SNR. Additionally, the contact response of the output power normalized with respect to that when there is no polymer contact, i.e. $h_{press} = 0$, is shown in Fig. 3(e). The result shows that greater N results in relatively sharper light losss. Using these findings, the parameters that maximize f_{obj} were determined, and as shown in Fig. 3(f), the optimal values were found to be $(R_b, N) = (0.5\ mm, 3)$.

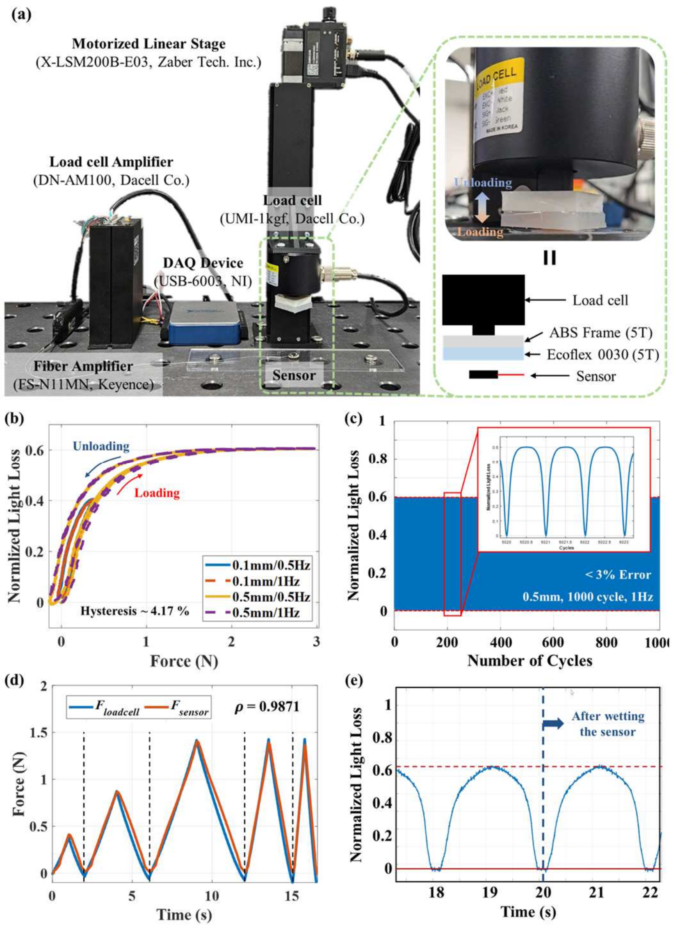

Figure 4. (a) Test-bed for sensor performance evaluation. Force and light intensity were measured during the loading/unloading process using motorized linear stage. Results of the (b) hysteresis, (c) repeatability, and (d) force estimation accuracy. (e) Consistent performance of the sensor even the sensor was wetted by water.

C. Sensor Fabrication

A base frame for weaving the optical fiber was 3D printed using a flexible thermoplastic polyurethane (TPU). The optical fiber (Eska, SH-1001.1) with a diameter of 250 µm was woven onto the base frame by passing the fiber alternately over and under the rods in a weaving pattern, which is repeated three times to create a stable structure, as shown in Fig. 1(a). After the weaving process, a fabric layer coated with polymer (Smooth-On, Ecoflex 00-30) was placed on top of the woven optical fiber. In this study, a commonly used polymer with a low modulus was utilized to achieve high sensitivity, making it suitable for detecting small forces. However, as a higher modulus of the polymer layer results in smaller deformation, it becomes more effective for measuring larger forces. This indicates that by coating the sensor with polymers tailored to the desired sensitivity and measurement range, the sensor performance can be easily adjusted. The polymer-coated fabric enhances the dynamic mechanical response of the sensor by improving the transmission of repetitive pressure, while the uncoated fabric serves as a stable backing layer. To secure the entire structure, the edges of the fabric layers and the base frame were stitched together using thread and a needle. The overall size of the fabricated sensor is approximately 10 mm in diameter and 2 mm in thickness, making it compact and lightweight. This design allows the sensor to be easily embedded into wearable applications, such as sleeves, without compromising flexibility or causing discomfort during use.

III. Sensor Performance

A. Test-bed Setup

To evaluate the performance of the sensor, a test-bed was constructed using a motorized linear stage (X-LSM200B-E03, Zaber Tech. Inc.) and a load cell (UMI-1kgf, Dacell Co.) to measure applied forces as shown in Fig. 4(a). The load cell was mounted on the motorized stage, and the sensor was positioned directly beneath it to ensure precise force application. A frame with a 5 mm-thick layer of polymer (Ecoflex 00-30) was placed beneath the load cell. A optical fiber amplifier (FS-N11MN, Keyence) was employed to deliver the light and to measure the light output. The entire system was controlled and monitored using a Data Acquisition (DAQ) device (USB-6003, National Instruments).

B. Performance Evaluation

Fig. 4(b) illustrates the experimental results obtained by applying forces to the sensor under varying loading/unloading depths and speeds. Specifically, the sensor was tested at depths of 0.1 mm and 0.5 mm and frequencies of 0.5 Hz and 1 Hz. These frequencies were selected as representative conditions corresponding to the typical motion bandwidth of upper-limb activities, which generally occur within a maximum range of 2 Hz. The tests were designed to evaluate the sensor's response to different mechanical inputs and to observe the behavior of scattering-based light loss under applied forces. The results demonstrated that the sensor exhibited high sensitivity to forces within the range of 3 N, with a clear and consistent response across all test conditions. Regardless of the pressing depth or speed, the light loss followed a similar trend, indicating that the sensor output is largely independent of these parameters. Furthermore, the hysteresis of the sensor was measured at just 4.17%, highlighting its excellent stability and repeatability during cyclic loading/unloading.

Fig. 4(c) shows the results of a durability test in which the sensor was subjected to 1,000 cycles of loading/unloading at a depth of 0.5 mm and a frequency of 1 Hz. Even after repeated cyclic presses, the sensor maintained consistent performance, with an error of only 3%. This minimal error demonstrates the robustness and reliability of the sensor, making it well-suited for applications requiring prolonged and repetitive use. Also, as shown in Fig. 4(d), the sensor was calibrated to evaluate its ability to accurately follow the applied force. By varying the pressing depth and speed during loading and unloading, results demonstrated that it could estimate the force with high accuracy, achieving a correlation coefficient of over 98%. These results validate the sensor capability to provide accurate and stable measurements under diverse operating conditions. Finally, water was applied to the sensor during loading and unloading to verify its sweat-proof properties, as shown in Fig. 4(e). Even when the sensor was slightly wet, it maintained its performance because the optical fiber contacts the polymer rather than the skin, and the polymer layer provides partial waterproofing.

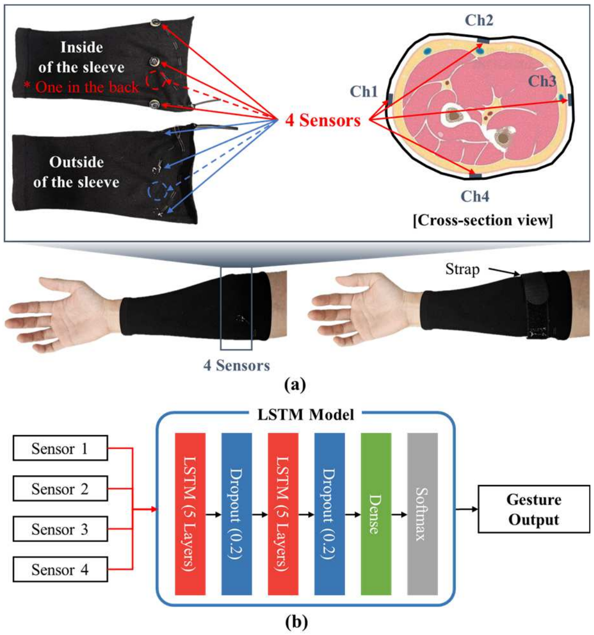

Figure 5. (a) Four sensors were embedded on the sleeve of the forearm with same distance. After wearing the sleeve, initial pressure was applied using strap to fix the system. (b) Schematic of LSTM neural network model for hand gesture recognition.

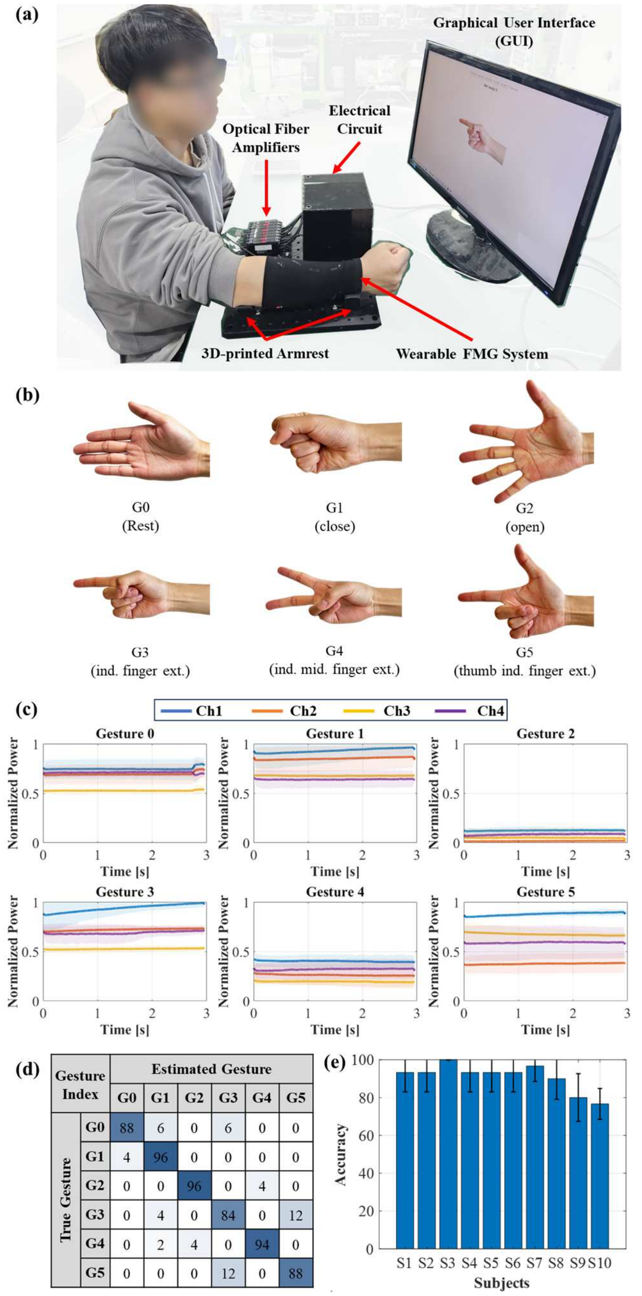

Figure 6. (a) Test bed and (b) six gestures: G0 (Rest), G1 (close), G2 (open), G3 (index finger extension), G4 (index middle finger extension) G5 (thumb index finger extension) (c) Averaged raw data of each gesture and channel. (d) Confusion matrix (unit: %) of the user test and (e) individual accuracy of each subject.

However, if the sensor is fully submerged in water, its performance may be affected due to changes in the refractive index, which is fundamental to its working principle.

IV. Wearable FMG System

A. Wearable System Design and Fabrication

After evaluating the performance of the sensor, a wearable FMG system was developed for hand gesture and grasping force estimation. Four sensors were embedded at equal intervals on the forearm section of a sleeve as shown in Fig. 5(a). The bottom layer used in Fig. 1(a) was replaced to the sleeve layer, sewing the sensors directly into the sleeve layer. This method enabled the integration of thin and flexible sensors without relying on complex techniques. After wearing the sleeve, a strap was used to provide appropriate initial pressure and to properly secure the position of the sensors.

B. Hand Gesture Recognition (User Test)

To verify the accuracy and performance of the wearable FMG system, a user test was conducted in which participants performed six hand gestures, as shown in Fig. 6(b). These were then detected and classified by the neural network (NN) based on the sensor data from the FMG system. 10 healthy male subjects participated the user test, and their average age was 25.67 ± 1.66. The subjects were guided to sit on a chair and wear the FMG system on their convenient arm. The arm is then placed on the armrest for their comfort throughout the experiment. The user was instructed to follow instructions displayed on the graphical user interface (GUI) of the monitor as shown in Fig. 6(a). The first stage for collecting data for training NN involves a total of five measurement sets, with each set consisting of five repetitions for each of the six gestures. Each gesture was performed for 3 seconds, and the order of all gestures was randomized. To prevent fatigue, a 3-second break was provided between gestures, and a 15-minute rest period was given after completing each set. Subsequently, the data was used to train an LSTM model, resulting in the optimal model for each subject as shown in Fig. 5(b). Finally for the final stage to evaluate the trained model, the six gestures were randomly displayed on the GUI five times each similar to the process of obtaining training data. Participants were instructed to perform the prompted gesture. Based on the sensor data of FMG system, the model predicts the hand gesture which is then compared with the actual hand gesture.

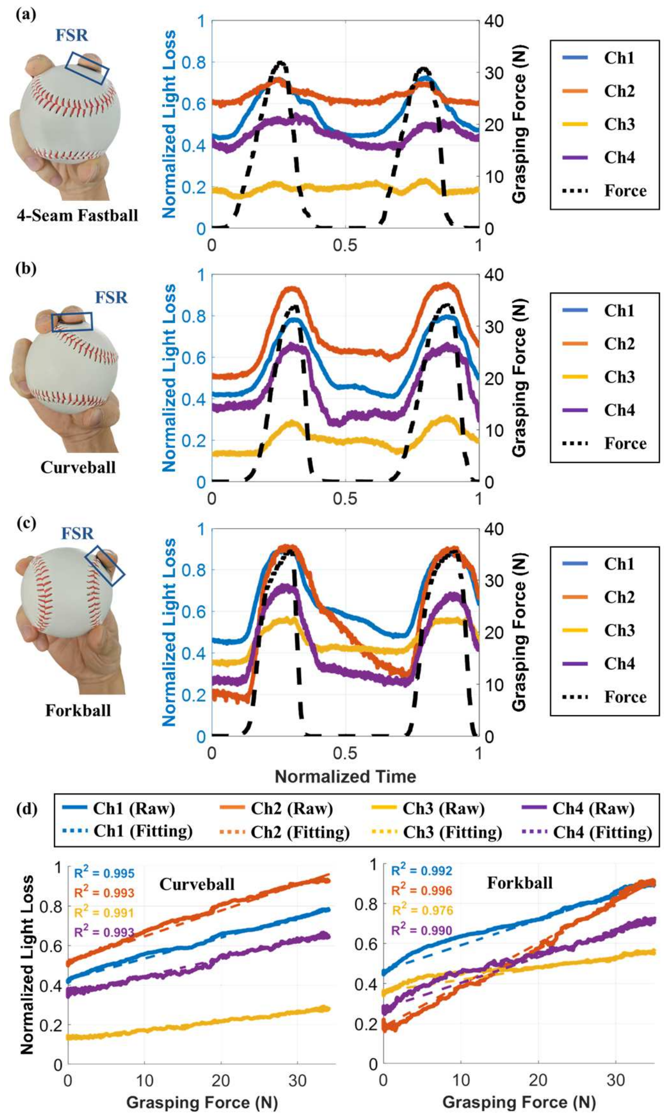

Figure 7. Grasping force and FMG data trends for different baseball grips: (a) 4-seam fastball, (b) curveball, and (c) forkball. (d) Normalized light loss trends in response to grasping force for curveball and forkball grips

For each gestures, the measured raw data of four sensors integrated in the FMG system was plotted, as seen in Fig. 6(c). The solid lines represent the mean values and the shaded region indicate the standard deviations. It can be observed that the four-channel data for the six gestures exhibit distinct patterns, making them sufficiently distinguishable. The performance of the hand gesture detection by the LSTM model is shown in Fig. 6(d) and (e). When examining the accuracy for each subject, most demonstrated high accuracy of about 95%. However, subjects S9 and S10 showed low average accuracy, of about 80% and 78%. This discrepancy is likely due to individual differences in muscle mass and body shape, even though the same wearable sleeve system was used, resulting in reduced accuracy for specific subjects. However, from the experimental results we can understand that even with only four channels, the FMG system was capable of detecting hand gestures with high accuracy and sensitivity, which can further allow distinction of more than six gestures.

C. Grasping Force Estimation

The FMG system was not only evaluated for hand gesture detection but also to determine whether it could estimate grasping force. To evaluate this feasibility of force estimation, the relationship between grasping force and FMG sensor data was analyzed across different grasping postures to hold a baseball. The baseball was grasped using three different grips- 4-seam fastball, curveball, and forkball- with an approximate grasping force of 30 N, while the data from four FMG channels were monitored. For each grip, the grasping force was measured twice by using a force-sensitive resistor (FSR) placed on the index finger as shown in Fig. 7(a)-(c).

The results show that the normalized light loss at the initial stage varies among the three different grips, indicating that the grip types can be distinguished, similar to hand gesture recognition. Additionally, it was observed that the values of the four FMG channels increase and decrease collectively as the grasping force increases and decreases. The trends in channel-specific data during the grasping process for the curveball and forkball grips, based on the grasping force, are shown in Fig. 7(d). It was observed that most of the channels exhibit high linearity with values exceeding 0.99 for both curveball and forkball grips. This indicates that not only can the grip type be distinguished, but the grasping force associated with each grip can also be reliably predicted.

V. Conclusion and Discussion

This study introduced a novel FMG sensor with a woven optical fiber structure for accurate and reliable force sensing in wearable haptic applications. The compact, highly flexible 2 mm-thick sensor integrates seamlessly into wearable systems and provides stable, repeatable force measurements with low hysteresis over 1,000 loading cycles. Its strong resistance to electromagnetic interference and sweat enhances practical usability. A wearable system achieved about 91% accuracy in classifying six hand gestures using an LSTM model and demonstrated high correlation in grasping force estimation across grip types, confirming its potential for dynamic force measurement and interactive haptics.

While the proposed FMG sensor demonstrated strong performance in force sensing and gesture recognition, certain limitations remain. First, the system requires subject-specific calibration due to inter-individual variations in forearm musculature, which influences the muscle deformation pattern and consequently the optical response. Second, the force estimation exhibits nonlinearity and increased error during unloading phases, likely due to soft tissue recovery dynamics and residual hysteresis. Although the current design achieves sufficient repeatability under controlled conditions, these factors must be addressed for broader applicability. Future work will focus on improving model generalization to minimize the need for per-user retraining and on developing a sensing strategy capable of capturing both loading and unloading behaviors with higher accuracy. Additionally, the integration of individual finger joint angle estimation will be explored to further enhance gesture recognition resolution for advanced haptic and HRI applications.

REFERENCES

[1] J. Jeong et al., "Soft Wearable Robot With Shape Memory Alloy (SMA)-Based Artificial Muscle for Assisting With Elbow Flexion and Forearm Supination/Pronation," *IEEE Robotics and Automation Letters*, vol. 7, no. 3, pp. 6028-6035, July 2022.

[2] C. Chung, K. Hyeon, J. Jeong, D. -Y. Lee and K. -U. Kyung, "Origami-Inspired Wearable Robot for Shoulder Abduction Assistance: A Double-Petal Mechanism Utilizing Shape Memory Alloy Actuators," *IEEE Robotics and Automation Letters*, vol. 9, no. 2, pp. 1484-1491, Feb. 2024.

[3] E. Mastinu et al., "Neural feedback strategies to improve grasping coordination in neuromusculoskeletal prostheses," *Sci. Rep.*, vol. 10, no. 1, p. 11793, 2020.

[4] K. Hyeon, C. Chung, J. Ma and K. -U. Kyung, "Lightweight and Flexible Prosthetic Wrist With Shape Memory Alloy (SMA)-Based Artificial Muscle and Elliptic Rolling Joint," *IEEE Robotics and Automation Letters*, vol. 8, no. 11, pp. 7849-7856, Nov. 2023.

[5] D. Blana, T. Kyriacou, J. M. Lambrecht, and E. K. Chadwick, "Feasibility of using combined EMG and kinematic signals for prosthesis control: A simulation study using a virtual reality environment," *J. Electromyogr. Kinesiol.*, vol. 29, pp. 21–27, 2016.

[6] A. Dwivedi, Y. Kwon, and M. Liarokapis, "EMG-based decoding of manipulation motions in virtual reality: Towards immersive interfaces," in *2020 IEEE International Conference on Systems, Man, and Cybernetics (SMC)*, 2020.

[7] Y. Desmarais, D. Mottet, P. Slangen, and P. Montesinos. "A review of 3D human pose estimation algorithms for markerless motion capture." *Computer Vision and Image Understanding*, 2021.

[8] M. Caeiro-Rodríguez, I. Otero-González, F. A. Mikic-Fonte, and M. Llamas-Nistal. "A systematic review of commercial smart gloves: Current status and applications." *Sensors*, vol. 21, no. 8, 2021.

[9] D. W. O. Antillon, C. R. Walker, S. Rosset and I.A. Anderson, "Glove-based hand gesture recognition for diver communication." *IEEE Transactions on Neural Networks and Learning Systems*, vol.34, no.12, pp. 9874-9886, 2022.

[10] M. Montazerin, E. Rahimian, F. Naderkhani, S. F. Atashzar, S. Yanushkevich, and A. Mohammadi, "Transformer-based hand gesture recognition from instantaneous to fused neural decomposition of high-density EMG signals," *Sci. Rep.*, vol. 13, no. 1, p. 11000, 2023.

[11] A. Moin, A. Zhou, A. Rahimi, A. Menon, S. Benatti, G. Alexandrov, S. Tamakloe, J. Ting, N. Yamamoto, Y. Khan et al., "A wearable biosensing system with in-sensor adaptive machine learning for hand gesture recognition," *Nature Electronics*, vol. 4, no. 1, pp. 54–63, 2021.

[12] Q. Hu, G. A. Azar, A. Fletcher, S. Rangan and S. F. Atashzar, "ViT-MDHGR: Cross-Day Reliability and Agility in Dynamic Hand Gesture Prediction via HD-sEMG Signal Decoding," *IEEE Journal of Selected Topics in Signal Processing*, vol. 18, no. 3, pp. 419-430, April 2024.

[13] M. R. U. Islam and S. Bai, "Effective multi-mode grasping assistance control of a soft hand exoskeleton using force myography," *Front. Robot. AI*, vol. 7, p. 567491, 2020.

[14] S. An, J. Feng, E. Song, K. Kong, J. Kim, and H. Choi, "High-accuracy hand gesture recognition on the wrist tendon group using pneumatic mechanomyography (pMMG)," *IEEE Trans. Industr. Inform.*, pp. 1–12, 2023.

[15] M. K. Gomes, W. H. A. da Silva, A. Ribas Neto, J. Fajardo, E. Rohmer, and E. Fujiwara, "Detection of hand poses with a single-channel optical fiber force myography sensor: A proof-of-concept study," *Automation*, vol. 3, no. 4, pp. 622–632, 2022.

[16] Y. L. Harvill, T. G. Zimmerman, and J.-J. G. Grimaud, "Motion sensor which produces an asymmetrical signal in response to symmetrical movement," U.S. Patent 5,097,252, Mar. 17, 1992.

[17] Y. Li, H. Di, Y. Xin, and X. Jiang, "Optical fiber data glove for hand posture capture," *Optik*, vol. 233, p. 166603, Feb. 2021

[18] X. Zhang, C. Wang, T. Zheng, H. Wu, Q. Wu, and Y. Wang, "Wearable optical fiber sensors in medical monitoring applications: A review," *Sensors*, vol. 23, no. 15, p. 6671, Jul. 2023

[19] S. Zhang, T. Li, G.-W. Lu, and Y. Sunami, "Ultra-flexible perceptual photonic-skin by using optical fiber as artificial mechanoreceptor," *Microsyst. Technol.*, vol. 25, pp. 4341–4347, 2019

[20] Z. G. Xiao and C. Menon, "A review of Force Myography Research and development," *Sensors*, vol. 19, no. 20, p. 4557, Oct. 2019.

[21] C. Chung, H. Mun, S. F. Atashzar and K. -U. Kyung, "A Novel Design of Thin Flexible Force Myography Sensor Using Weaved Optical Fiber: A Proof-of-Concept Study," *2024 21st International Conference on Ubiquitous Robots (UR)*, New York, NY, USA, 2024, pp. 1-6.

[22] H. Mun, D. S. D. Cortes, J.-H. Youn, and K.-U. Kyung, "Multi-degree-of-freedom force sensor incorporated into soft robotic gripper for improved grasping stability," *Soft Robot.*, vol. 11, no. 4, pp. 628-638, Aug. 2024

[23] R. T. Schermer and J. H. Cole, "Improved Bend Loss Formula Verified for Optical Fiber by Simulation and Experiment," *IEEE Journal of Quantum Electronics*, vol. 43, no. 10, pp. 899-909, Oct. 2007.